

## 3D MULTISTAGE COMPUTATIONS OF TURBINE FLOWS USING DIFFERENT STATE EQUATIONS

ANDREY V. RUSANOV<sup>1</sup>, SERGEY V. YERSHOV<sup>1</sup>,  
PIOTR LAMPART<sup>2</sup>, JERZY ŚWIRYDCZUK<sup>2</sup>  
AND ANDRZEJ GARDZILEWICZ<sup>2</sup>

<sup>1</sup>*Institute of Mechanical Engineering Problems,  
Ukrainian National Academy of Sciences,  
2/10 Pozharsky, 61046 Kharkov, Ukraine  
rusanov@ipmach.kharkov.ua  
Flower ltd., Kharkov, Ukraine  
flower@flower3d.org*

<sup>2</sup>*Institute of Fluid Flow Machinery, Polish Academy of Sciences,  
Fiszera 14, 80-952 Gdansk, Poland  
lampart@imp.gda.pl*

(Received 30 August 2001; revised manuscript received 16 August 2002)

**Abstract:** The paper describes the implementation of a modified state equation for perfect gas and Tammann equation into a 3D RANS solver FLOWER. In the modification the specific heats are assumed as linear functions of temperature. A 5-stage LP (low pressure) steam turbine is calculated, and the comparison of results for constant and variable specific heats is illustrated. The modification significantly improves the correctness of determination of thermodynamic parameters in the entire flow region, especially in the exit stage.

**Keywords:** 3D RANS model, state equation, low pressure steam turbine

### 1. Introduction

Navier-Stokes solvers with turbomachinery applications usually operate on the thermal and caloric equation of perfect gas. This approach is relatively well-grounded for one-component one-phase throughflow, which in steam turbines is believed to take place in high and intermediate pressure turbine stages where the steam is superheated. The approach requires determination of an individual gas constant and setting appropriate values of specific heats, or specific heat ratio. Unless the range of variation of flow parameters is too wide, the scheme will converge and a solution will be obtained. The perfect gas equations can not be accepted for solving the flow in low pressure turbines, both in the region where the steam is still superheated

and, especially, for the exit stages of large power turbines where the steam expands across the saturation line, changing dramatically its properties. For long, a common practice of CFD research engineers was to perform calculations of low pressure turbines individually for each stage, using the perfect gas equation and changing the constant values of individual gas constant and specific heat ratio from stage to stage.

The ideal solution to the above problem would be to use steam tables to generate correct values of thermodynamic parameters of steam. However, it involves increased computational costs, possibly even as large as two orders of magnitude. Therefore, in their code, Chmielniak *et al.* [1], Wróblewski [2] propose to use the virial equation of Vukalovich and Rivkin [3] for superheated and subcooled steam, whereas Dykas [4] proposes the application of some kind of virial equation, that is a so-called local real gas equation of state. In general, the virial equation reads as  $pv/RT = z(T,p)$  or  $pv/RT = z(T,v^{-1})$ , where the function  $z$  is a polynomial with respect to pressure or inverse specific volume, and the polynomial coefficients are functions of temperature only and can be found from approximation of thermodynamic properties of water and steam IAPWS'97, see Wagner *et al.* [5]. The computational costs of flow solver using a virial equation are increased by a factor of 3–8 times over the solver with the perfect gas equation [4]. The authors [1, 2, 4] use a 3D Euler solver with additional conservation equations for the liquid phase, drawing also on the classical nucleation theory for the formation of the liquid phase.

The concept proposed in this paper is still a simpler modification of the perfect gas equation and the Tammann equation, which makes the specific heats variable as a linear function of temperature, while keeping the individual gas constant unchanged. The effect of the introduced modification on the distribution of thermodynamic parameters is illustrated using a computational example of a 5-stage LP steam turbine.

## 2. RANS equations

In the code FLOWER developed by Yershov and Rusanov [6], 3D viscous compressible flow through a turbine/compressor stage can be described by a set of unsteady Reynolds-averaged Navier-Stokes equations written in a curvilinear body-fitted coordinate system  $(\xi, \eta, \zeta)$ , rotating with an angular speed  $\varpi$ :

$$\frac{\partial QJ}{\partial t} + \frac{\partial(E\xi_x + F\xi_y + G\xi_z)J}{\partial \xi} + \frac{\partial(E\eta_x + F\eta_y + G\eta_z)J}{\partial \eta} + \frac{\partial(E\zeta_x + F\zeta_y + G\zeta_z)J}{\partial \zeta} = HJ, \quad (1)$$

where

$$Q = \begin{bmatrix} \rho \\ \rho u \\ \rho v \\ \rho w \\ \rho h \end{bmatrix}; \quad H = \begin{bmatrix} 0 \\ 2\rho\nu\varpi + \rho\varpi^2 r_x \\ -2\rho u\varpi + \rho\varpi^2 r_y \\ 0 \\ 0 \end{bmatrix}; \quad E = \begin{bmatrix} \rho u \\ \rho u^2 + p - \tau_{xx} \\ \rho u v - \tau_{xy} \\ \rho u w - \tau_{xz} \\ (\rho h + p)u - u\tau_{xx} - \nu\tau_{xy} - w\tau_{xz} + q_x \end{bmatrix};$$

$$F = \begin{bmatrix} \rho\nu \\ \rho w\nu - \tau_{xy} \\ \rho\nu^2 + p - \tau_{yy} \\ \rho\nu w - \tau_{yz} \\ (\rho h + p)\nu - u\tau_{xy} - \nu\tau_{yy} - w\tau_{yz} + q_y \end{bmatrix}; G = \begin{bmatrix} \rho w \\ \rho w\nu - \tau_{xz} \\ \rho\nu w - \tau_{yz} \\ \rho w^2 + p - \tau_{zz} \\ (\rho h + p)w - u\tau_{xz} - \nu\tau_{yz} - w\tau_{zz} + q_z \end{bmatrix};$$

$$h = \varepsilon + \frac{u^2 + \nu^2 + w^2 - \varpi^2 r^2}{2} + \text{const.}; \quad q = -\lambda \nabla T;$$

$$\tau_{ij} = \tau_{m_{ij}} + \tau_{t_{ij}}; \quad \tau_{m_{ij}} = 2\mu_m(S_{ij} - S_{nn}\delta_{ij}/3); \quad \tau_{t_{ij}} = 2\mu_t(S_{ij} - S_{nn}\delta_{ij}/3) - 2\rho k\delta_{ij}/3.$$

The symbols  $\varepsilon$ ,  $p$ ,  $\rho$ ,  $u$ ,  $v$ ,  $w$  denote the internal energy, pressure, density and components of the velocity,  $T$  – temperature,  $\tau_{m_{ij}}$ ,  $\tau_{t_{ij}}$ ,  $\tau_{ij}$  are the molecular, turbulent and total viscous stress,  $S_{ij}$  – mean strain-rate tensor,  $\mu = (\mu_m + \mu_t)$  – effective (molecular + turbulent) viscosity,  $q$  – heat flux,  $\lambda = (\lambda_m + \lambda_t) = c_p(\mu_m/\text{Pr}_m + \mu_t/\text{Pr}_t)$  – effective (molecular + turbulent) heat conductivity,  $\text{Pr}_m$ ,  $\text{Pr}_t$  – molecular and turbulent Prandtl numbers.

The governing equations are supplemented with two eddy-viscosity models – the algebraic model of Baldwin-Lomax [7] and the two-equation Menter SST model [8]. In the former, the boundary layer is divided into two domains – an inner and outer layer. The turbulent viscosity in the inner region is calculated from the Prandtl concept of mixing length, whereas in the outer region of the boundary layer is defined by the modified Clauser formula:

$$\mu_t = \rho l^2 \Omega \quad \text{or} \quad \mu_t = \alpha C_{CP} \rho F_{WK} F_K, \quad (2)$$

where  $\Omega$  is the vorticity (absolute value),  $l$  – mixing length,  $\alpha$  and  $C_{CP}$  are constants,  $F_{WK}$  is the wake function,  $F_K$  is the Klebanoff intermittency factor. The flow is assumed turbulent if at some point of the boundary layer profile the eddy viscosity calculated as prescribed above is 14 time larger than the molecular viscosity of undisturbed flow. Otherwise, the boundary layer is thought to be laminar at this section.

In the Menter shear stress transport model, the standard  $k$ - $\omega$  model is activated in the near wall region, and then switched to the  $k$ - $\varepsilon$  model in the wake region of the boundary layer and free shear layers. In order to more adequately predict strong adverse pressure gradient flows, the eddy viscosity is redefined so as to guarantee the proportional relationship between the principal turbulent shear stress and the turbulent kinetic energy in the boundary layer. A number of test cases given by Menter [8], including Driver's adverse pressure gradient flow, backward-facing step, NACA airfoil and transonic bump flows, show that the SST model yields a substantially better agreement with the experimental data, compared to those of other turbulence models. The Menter SST turbulence model in  $k$ - $\omega$  formulation can be written as:

$$\frac{\partial U}{\partial t} + \frac{\partial R_i}{\partial x_i} = G - D + L, \quad (3)$$

where

$$U = \begin{bmatrix} \rho k \\ \rho \omega \end{bmatrix}; \quad R_i = \begin{bmatrix} \rho k - (\mu + \sigma_k \mu_t) \frac{\partial k}{\partial x_i} \\ \rho \omega - (\mu + \sigma_\omega \mu_t) \frac{\partial \omega}{\partial x_i} \end{bmatrix}; \quad G = \begin{bmatrix} \tau_{ij} S_{ij} \\ \gamma \frac{\omega}{k} \tau_{ij} S_{ij} \end{bmatrix}; \quad D = \begin{bmatrix} \beta^* \rho \omega k \\ \beta \rho \omega^2 \end{bmatrix};$$

$$L = \left[ \begin{array}{c} 0 \\ 2(1-F_1) \frac{\rho\sigma_{\omega 2}}{\omega} \frac{\partial k}{\partial x_i} \frac{\partial \omega}{\partial x_i} \end{array} \right]; \quad \mu_t = \frac{\rho k / \omega}{\max[1; \Omega F_2 / (a_1 \omega)]},$$

where, in turn,  $k$  is the turbulent kinetic energy,  $\omega = \varepsilon/k\beta^*$  – specific dissipation rate,  $\mu_t$  – turbulent viscosity. Blending functions  $F_1$  (assuring smooth transition from the  $k$ - $\omega$  to the  $k$ - $\varepsilon$ , and assuming one in the sublayer and logarithmic region and gradually switching to zero in the wake region of the boundary layer) and  $F_2$  (assuring the proportional relationship between the principal turbulent shear stress and the turbulent kinetic energy in the boundary layer, and assuming one in the boundary layers and switching to zero in free shear layers) are:

$$\begin{aligned} F_1 &= \tanh \left\{ [\min(A_1; A_2)]^4 \right\}; \quad F_2 = \tanh \left\{ [\max(2B_1; B_2)]^2 \right\} \\ A_1 &= \max(B_1; B_2); \quad A_2 = \frac{4\rho\sigma_{\omega 2}k}{CD_{k\omega}y^2}; \quad B_1 = \frac{\sqrt{k}}{\beta^*\omega y}; \quad B_2 = \frac{500\mu}{\rho y^2 \omega}; \\ CD_{k\omega} &= \max \left( 2 \frac{\rho\sigma_{\omega 2}}{\omega} \frac{\partial k}{\partial x_i} \frac{\partial \omega}{\partial x_i}; 10^{-20} \right). \end{aligned}$$

A vector of constants  $\phi = [\sigma_k, \sigma_{\omega}, \beta, \gamma]$  in the SST model can be written:  $\phi = F_1\phi_1 + (1-F_1)\phi_2$ , where  $\phi_1$  is this vector in the  $k$ - $\omega$  model, and  $\phi_2$  in the  $k$ - $\varepsilon$  model written in  $k$ - $\omega$  formulation. The constants of the model are:  $a_1 = 0.31$  (Bradshaw constant),  $\sigma_{k1} = 0.85$ ,  $\sigma_{k2} = 1.0$ ,  $\sigma_{\omega 1} = 0.5$ ,  $\sigma_{\omega 2} = 0.856$ ,  $\beta^* = 0.09$ ,  $\beta_1 = 0.075$ ,  $\beta_2 = 0.0828$ ,  $\gamma_1 = 0.553$ ,  $\gamma_2 = 0.44$ .

The boundary conditions for the set of Equations (1) are: at the walls – no-slip and no heat flux; at the inlet – span-wise distribution of the total pressure, total temperature and flow angles at the inlet to the stage; at the exit – static pressure (either its span-wise distribution or a value at the mid-span with the radial equilibrium equation assumed). For the set of Equations (3), the boundary conditions are: at the walls –  $k = 0$ ;  $\omega = 60\mu_w/\rho_w\beta y^2$ ; at the inlet –  $k = 1.5(\text{Tu}U_{\infty})^2$ ;  $\omega = [\max(S\Omega, \Omega^2)]^{0.5}$ , where  $S = (S_{ij}S_{ij}/2)^{0.5}$ , Tu – inlet free-stream turbulence,  $\Omega$  – vorticity (absolute value), and the subscript  $w$  denotes values at the wall; at the outlet – values of  $k$  and  $\omega$  are extrapolated from the preceding cell centres. The computations for this paper are carried out in one blade-to-blade passage of each blade row, with the condition of spatial periodicity and mixing plane approach assumed.

### 3. State equations

Four cases are considered here:

1. thermally and calorically perfect gas

$$p = R\rho T; \quad i = \frac{\gamma}{\gamma-1} \frac{p}{\rho} + \text{const.}; \quad c_p, c_v, R, \gamma = \text{const.}; \quad (4)$$

2. thermally perfect, but calorically imperfect gas with variable specific heats

$$p = R\rho T; \quad i = \frac{\gamma}{\gamma-1} \frac{p}{\rho} + \text{const.}; \quad R = \text{const.}; \quad c_p, c_v, \gamma \neq \text{const.}; \quad (5)$$

$$c_v = c_{v0} + c_v^t(T - T_0), \quad c_p = c_{p0} + c_p^t(T - T_0); \quad c_{v0}, c_v^t, c_{p0}, c_p^t = \text{const.}, \quad c_v^t = c_p^t \neq 0;$$

3. Tammann equation with constant specific heats

$$p + p_0 = R\rho T; \quad i = \frac{\gamma}{\gamma-1} \frac{p + p_0}{\rho} + \text{const.}; \quad R, c_p, c_v, \gamma = \text{const.}; \quad (6)$$

4. Tammann equation with variable specific heats

$$p + p_0 = R\rho T; \quad i = \frac{\gamma}{\gamma-1} \frac{p+p_0}{\rho} + \text{const.}; \quad R = \text{const.}; \quad c_p, c_v, \gamma \neq \text{const.}; \quad (7)$$

$$c_v = c_{v0} + c_v^t(T - T_0), \quad c_p = c_{p0} + c_p^t(T - T_0); \quad c_{v0}, c_v^t, c_{p0}, c_p^t = \text{const.}, \quad c_v^t = c_p^t \neq 0.$$

In Equations (4)–(7) symbols  $p$ ,  $\rho$ ,  $T$ ,  $i$  denote pressure, density, temperature and enthalpy;  $p_0$ ,  $T_0$  are reference pressure and temperature;  $c_p$ ,  $c_v$  – specific heats at constant pressure and volume, respectively;  $R = c_p - c_v$  – individual gas constant;  $\gamma = c_p/c_v$  – specific heat ratio.

The above four cases are implemented in the code FLOWER. The numerical scheme is based on cell-centred finite-volume discretisation, Godunov-type upwind differencing, high resolution ENO scheme defined in characteristic variables, and  $\delta$  implicit operator, see Yershov [9], also Yershov *et al.* [10].

#### 4. LP turbine – geometry and operating conditions

A 5-stage LP turbine (part of a 360MW steam turbine) is studied in order to evaluate the effect of constant/variable specific heats on computed flow patterns. This drum-type reaction turbine has a radial inlet equipped with guide vanes and a radial outlet to the exhaust hood. Stators 2–5 and rotors 1–4 are shrouded and have typical labyrinth seals. Rotor 5 has unshrouded blades. Two regenerative extraction points are located downstream of stage 3 and 4. A schematic diagram of the tested turbine in meridional view is presented in Figure 1. The LP turbine was experimentally investigated for some range of load by Marcinkowski *et al.* [11]. These investigations are used here to define inlet/exit boundary conditions for the nominal load as:

- at the inlet: total temperature  $T_{0T} = 538\text{K}$ , total pressure  $P_{0T} = 5.166 \cdot 10^5 \text{Pa}$ , radial inflow;
- at the exit: static temperature  $T_2 = 317\text{K}$ , static pressure  $P_2 = 0.089 \cdot 10^5 \text{Pa}$ .

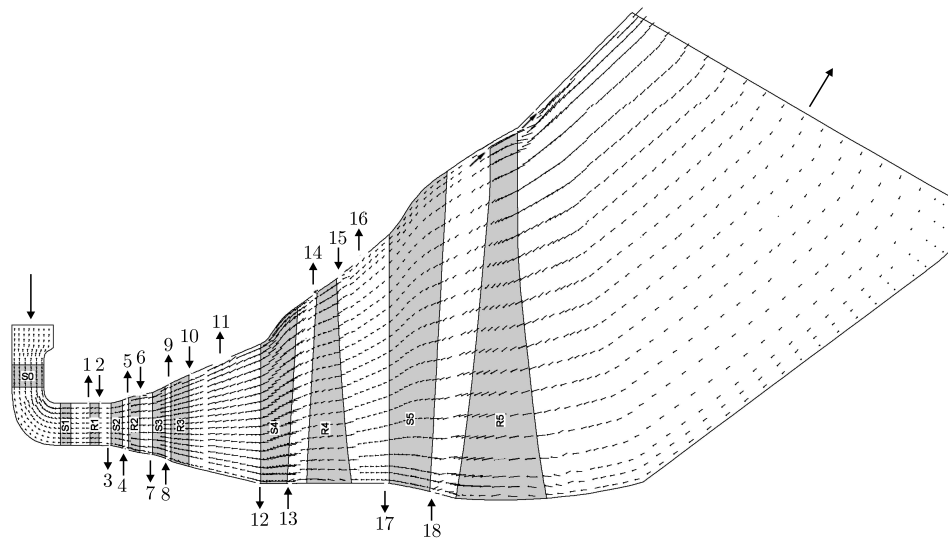


Figure 1. A 5-stage LP turbine in meridional view. Velocity vectors at mid blade-to-blade distance

Note here that the exit temperature is not a boundary condition for the solver but a value to receive a proper linear relationship for variation of the specific heats. The experimental investigations are also used in this paper to validate the obtained computational results behind the stage 3, 4 and 5 of the investigated turbine.

The computational domain extends on the region over unshrouded blade tips, which enables direct computation of leakage over this type of blades. The labyrinth seal regions of shrouded blades and windage passages are not in the computational domain, but a source/sink approach is used to enable injection or extraction of leakage streams to or from the main-flow passage, see Lampart *et al.* [12]. In this approach, the boundary conditions are mass flow rate, direction (two angles) and total temperature of streams injected into the blade-to-blade passage, and mass flow rates of extracted streams. This approach is also applicable to technological mass extractions. Figure 1 gives an indication of places at the endwalls referring to regenerative extractions and injection or extraction of leakage flows where source/sink-type boundary conditions are imposed. The needed mass flow rates and total temperatures of leakage flows and extractions are found from a 1D code, Gardzilewicz [13], and are collected for subsequent slots in Table 1 (due to lack of further information source stream angles are assumed to give the direction of the leakage jet re-entry normal to the endwalls).

**Table 1.** Source/sink parameters

Slot No.	1-2	3-4	5-6	7-8	9-10	11	12-13	14-15	16	17-18
Location	R 1	S 2	R 2	S 3	R 3	Extr.	S 4	R 4	Extr.	S 5
$G$ [kg/s]	$\pm 2.00$	$\pm 1.90$	$\pm 1.40$	$\pm 1.21$	$\pm 1.10$	-5.50	$\pm 0.54$	$\pm 1.10$	-5.00	$\pm 0.36$
$T_{0T}$ [K]	537.8	487.8	487.8	437.8	437.8	—	387.8	387.8	—	337.8

## 5. Computational results – comparison with available experimental data

Calculations of the 5-stage LP turbine were performed on a structured H-type grid of 1200000 cells in total refined near the endwalls, blade walls, trailing and leading edges. Two computational variants will be presented here. First, based on the thermally and calorically perfect gas with constant specific heats – in this case values of individual gas constant and specific heat ratio were assumed as from the inlet to the turbine that is in the region of superheated steam  $R = 450 \text{ kJ/kgK}$ ,  $\gamma = 1.31$ . Second, based on the thermally perfect and calorically imperfect gas with variable specific heats changing linearly as a function of temperature, with the specific heat ratio changing through the LP part from  $\gamma = 1.31$  to 1.05.

The already presented Figure 1 gives also a plot of velocity vectors through the meridional section of the turbine at the mid blade-to-blade distance, computed for the case of constant specific heats  $c_p, c_v = \text{const}$ . The similar plot for the case of variable specific heats will not exhibit considerable differences at this magnification, so will not be shown here. However, the differences in velocity fields can be quite important, which gives rise to differences in determination of mass flow rates in subsequent blade rows. Table 2 shows the comparison of computed (with constant and variable specific heats) mass flow rate in subsequent rows, as well as mass averaged pressure and temperature

downstream of subsequent stages. The computed pressures and temperatures are also compared with available experimental data downstream of stage 3, 4 and 5. The mass flow rates calculated with variable specific heats are consistently lower by 1–1.2 kg/s, that is by about 1%. Values of mass flow rate in subsequent rows can also be considered here a test for the correctness of the sink/source procedure. Mass flow rates of most leakage flows are determined correctly, which can be proved by subtracting respective numbers from Table 2 and comparing them with Table 1. The balance of mass flow rates at the inlet and exit shows that the solver slightly overestimates the amount of extracted steam:  $103.9 - 92.4$  (Table 2) =  $11.5 > 10.5 = 5.5 + 5.0$  (Table 1).

**Table 2.** Comparison of experimental and computed mass flow rate, pressure and temperature downstream of subsequent rows/stages

Stage	Row	Mass flow rate in row [kg/s]		Static pressure behind stage [bar]			Static temperature behind stage [K]		
		$c_p, c_v$ const.	$c_p, c_v$ var.	$c_p, c_v$ const.	$c_p, c_v$ var.	exp.	$c_p, c_v$ const.	$c_p, c_v$ var.	exp.
1	1	105	103.9	3.0	3.05	—	479.2	482.0	—
	2	105	103.9						
	3	103	101.9						
2	4	103	102	1.74	1.82	—	427.7	435.5	—
	5	103.5	102.4						
3	6	103.7	102.5	0.724	0.785	0.799	355.8	382.5	371.2
	7	103.7	102.5						
4	8	98.5	97.3	0.315	0.348	0.349	299.8	350.2	346.4
	9	98.0	96.8						
5	10	93.2	92	0.0835	0.0825	0.083	229.0	312	314.8
	11	93.6*	92.4*						

\* Mass flow rate of tip leakage over shrouded rotor blades included

The two methods of calculation yield different pressure drops across each stage. For first four stages the method of constant specific heats gives slightly higher pressure drops. For the exit stage the pressure drop is considerably larger for the case of variable specific heats. The comparison with experimental data reveals that only the case of variable specific heats yields good pressure predictions downstream of stage 3, 4 and 5. A similar situation is for temperature. The comparison of static temperature contours in meridional view at mid blade-to-blade distance in computations with constant and variable specific heats is shown in Figure 2. The application of constant specific heats can lead to unphysical results, such as 229K downstream of stage 5. Certainly, the observed differences in determination of temperature and pressure fields in the two methods of calculation lead to differences in determination of enthalpies, power and efficiency of subsequent stages, especially of the exit stage.

Another possibility for computations with constant specific heats that can be discussed here is to assume values of individual gas constant and specific heat ratio as an average value from the inlet and exit. This method is however not recommended for a 5-stage LP turbine as it does not solve the flow properly neither in the region

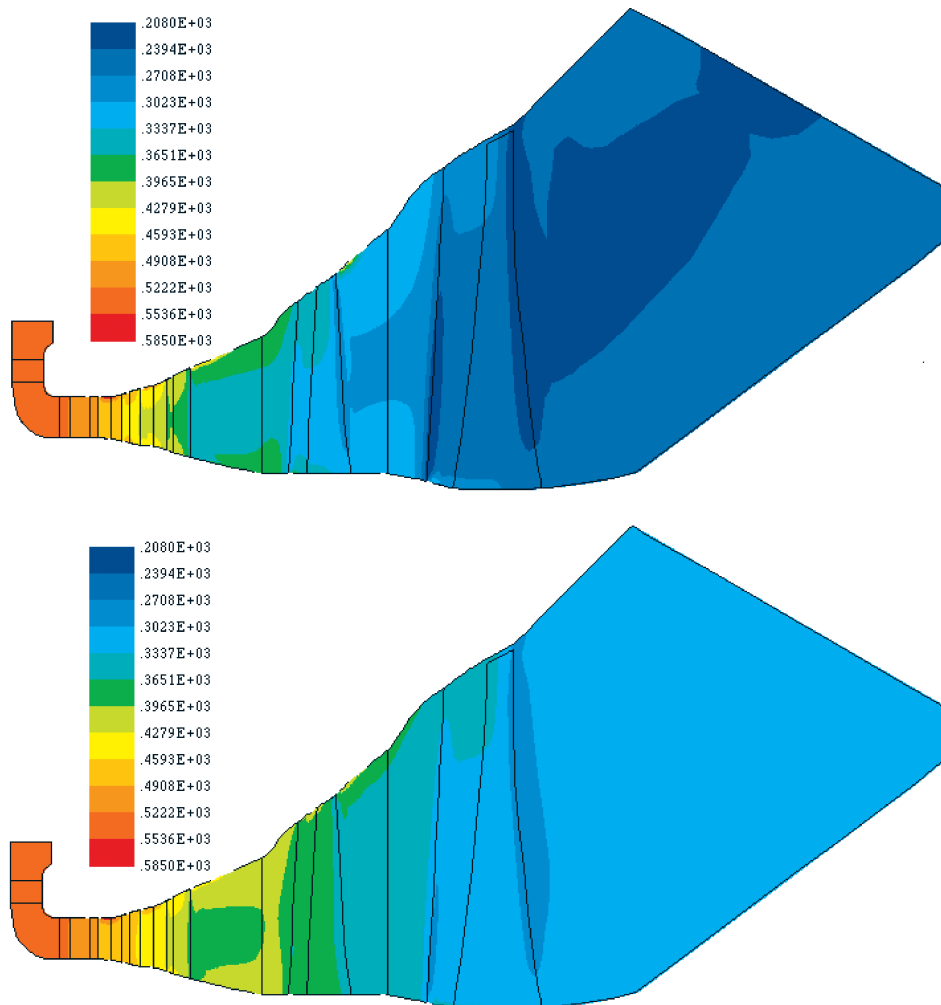


**Figure 2.** Comparison of static temperature contours in meridional view at mid blade-to-blade distance for  $c_p, c_v = const.$  (top) and  $c_p, c_v = var.$  (bottom)

of superheated nor in the region of wet steam. Still preserving the specific heats constant, an alternative is to perform calculations of each turbine stage individually, changing the specific heat ratio from stage to stage. This approach, however, disposes of the main advantage of multi-stage computations over single-cascade or single-stage computations, that is the possibility to pass flow parameters between the stages and allow the mixing processes generated in one stage to be completed or continued in the next stage (stages). Also single-stage computations would require boundary conditions for each stage which have to be provided from a 1D solver or from pressure/temperature measurements in stage-to-stage gaps. Then, most likely, another possibility is lost that the computations can be verified by the experimental investigations in the stage-to-stage gaps. This is usually due to a simple fact that there are no other sections available that were measured and not assumed as sections where computational boundary conditions are imposed.

In view of that fact, multi-stage computations with variable specific heats enable true comparison of numerical and experimental results. This comparison for spanwise pitch-average distribution of total and static pressure as well as meridional and swirl angle behind the stage 3, 4 and 5 is presented in Figure 3. The figure exhibits a relatively good agreement between the computed and measured results for all tested flow parameters. The comparison of measured and computed swirl angle is especially convincing.

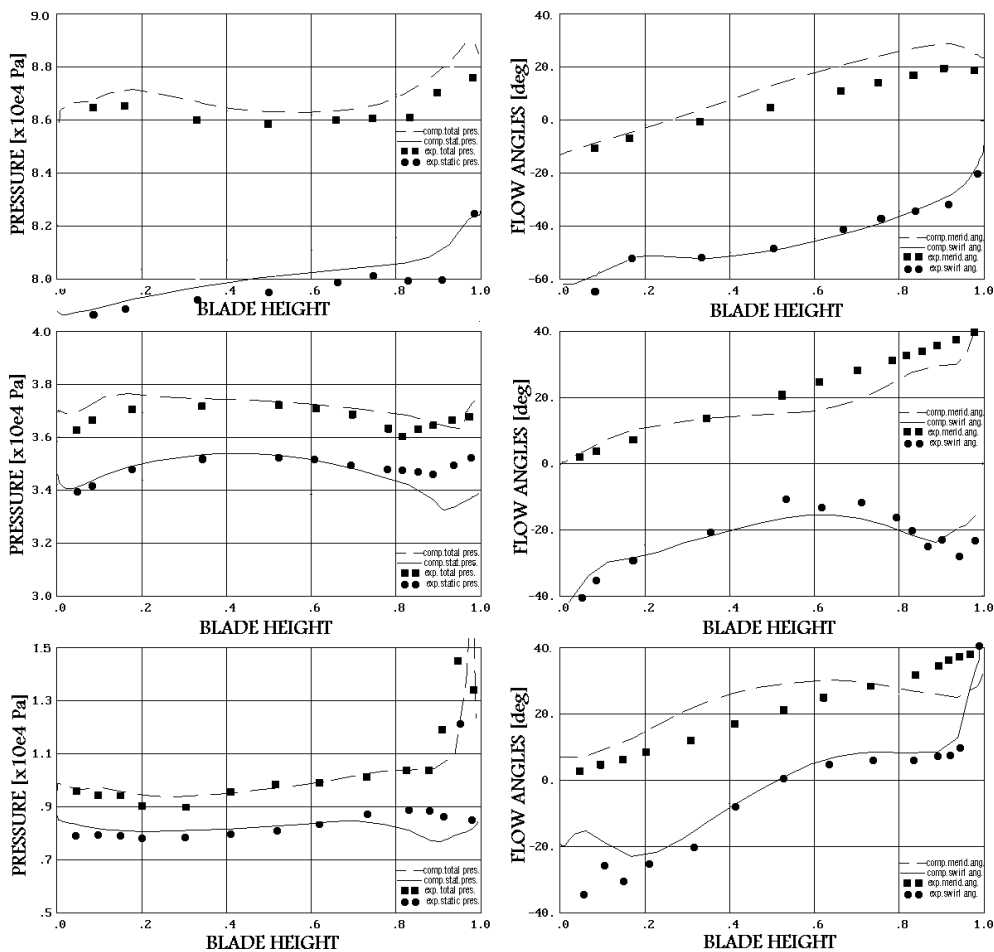


**Figure 3.** Comparison of experimental and computational ( $c_p, c_v = var.$ ) total and static pressure (left), meridional and swirl angle (right), downstream of stage 3 (top), 4 (centre), 5 (bottom)

## 6. Conclusions

A modified perfect gas equation and Tammann equation with variable specific heats changing as linear functions of temperature are implemented in a 3D RANS solver FLOWER for turbomachinery applications. A 5-stage LP turbine is calculated using a multi-stage approach and two variants of state equations – thermally and calorically

perfect gas with constant specific heats, and thermally perfect but calorically imperfect gas with variable specific heats. It is shown that only the latter variant provides correct determination of thermodynamic parameters. The distributions of pressures and flow angles in stage-to-stage gaps of a 5-stage LP steam turbine computed for the case of variable specific heats seem to reproduce the measured data relatively well.

### References

- [1] Chmielniak T J, Wróblewski W and Dykas S 1997 *Archives of Thermodynamics* **18** 99
- [2] Wróblewski W 2000 *Turbulence* **6-7** 209
- [3] Vukalovich M P and Rivkin C L 1969 *Teploenergetika* **3** 60 (in Russian)
- [4] Dykas S 2001 *TASK Quart.* **4** (4) 519
- [5] Wagner W, Cooper J R, Dittmann A, Kijima J, Kretzschmar H-J, Kruse A, Oguchi K, Sato H, Stocker I, Sifner O, Takaishi Y, Tanishita I, Trubenbach J and Willkommen Th 2000 *Trans. ASME, J. Engng. Gas Turbines Power* **122** 150
- [6] Yershov S V and Rusanov A V 1996 *The Application Package FLOWER for the Calculation of 3D Viscous Flows Through Multi-stage Turbomachinery*, Certificate of State Registration of Copyright, Ukrainian State Agency of Copyright and Related Rights
- [7] Baldwin B S and Lomax H 1978 *AIAA Paper* **78-257**
- [8] Menter F R 1994 *AIAA J.* **32** (8) 1598
- [9] Yershov S V 1994 *Math. Modelling* **6** (11) 58 (in Russian)
- [10] Yershov S V, Rusanov A V, Gardzilewicz A, Lampart P and Świryczuk J 1998 *TASK Quart.* **2** (2) 319
- [11] Marcinkowski S, Gardzilewicz A and Gluch J 1999 *Rep. Diagnostyka Maszyn* **11/99** (in Polish)
- [12] Lampart P, Gardzilewicz A, Yershov S V and Rusanov A V 2000 *ASME Paper* **IJPGC 2000-15004**
- [13] Gardzilewicz A 1984 *Rep. IMP PAN*, Gdansk, Poland **161/84** (in Polish)